

Optical Kerr nonlinearity in quantum-well microcavities: From polariton to dipolaritonH. Jabri¹ and H. Eleuch^{2,3}¹*Institut Supérieur de Biotechnologie, Université de Jendouba, Béja 9000, Tunisia*²*Department of Applied Physics and Astronomy, University of Sharjah, Sharjah 27272, United Arab Emirates*³*Institute for Quantum Science and Engineering, Texas A&M University, College Station, Texas 77843, USA*

(Received 29 June 2020; accepted 30 November 2020; published 16 December 2020)

In this paper, we investigate the nonlinear optical properties and photon correlations in a cavity containing quantum wells and interacting with a third-order nonlinear medium. More precisely, we study the interaction of the photonic Kerr nonlinearity with polariton and dipolariton quasiparticles in thermal environments. The optical bistability, the intensity spectrum, and the squeezing spectrum of the transmitted radiation are analyzed. It is shown that the regime of the bistability is reached in the dipolariton cavity faster than attained by the polariton system. Furthermore, the increase of the coupling with the wells reduces the squeezing. More interestingly, it turns out that the additional interactions arising in the dipolariton cavity, between direct and indirect excitons, slow down the variation of the squeezing. As a consequence, dipolaritons offer a greater margin of squeezed light than polaritons, and also than the $\chi^{(3)}$ medium in the absence of quantum wells. Moreover, the dipolariton system is found to be much more robust against the bath temperature in the weak-coupling regime.

DOI: [10.1103/PhysRevA.102.063713](https://doi.org/10.1103/PhysRevA.102.063713)**I. INTRODUCTION**

The optical Kerr effect is the nonlinear response of optical media to applied electromagnetic waves. Studying this effect is one of the basic topics in quantum and nonlinear optics as it is fundamental for the realization of many nonlinear optical processes [1,2]. The Kerr effect has several applications such as quantum nondemolition measurement [3,4], nonlinear and quantum controls of light fields [5], all-optical deterministic quantum logic [6,7], quantum bit regeneration [8], quantum state teleportation [9], and the generation of optical solitons [10,11]. The Kerr effect mainly appears in nonlinear dispersive materials owing to a third-order light-matter interaction [12]. Examples of devices generating nonlinear optical responses are the well-known nonlinear Fabry-Pérot resonators [13,14], structures with epitaxial Bragg reflectors [15,16], superlattices [17], and nonlinear interference filters [18].

Furthermore, and for several decades, semiconductor heterostructures have been widely studied both on the fundamental and applied aspects for the multitude and richness of the optical properties that they produce [19–21]. Semiconductor microcavities with quantum wells is a bright example that has highly contributed to the understanding and the development of these materials [22–28]. In this particular structure, it is possible to confine the electromagnetic field and electrons of the quantum well. This confinement increases the mutual interactions of the two fields and allows us to reach the strong-coupling regime. As a result, the fundamental excitation of this regime is a hybrid particle called a polariton, an exciton-photon mixed state [29]. This hybrid character leads to various observations and fascinating phenomena, having no classical counterpart, such as photon antibunching, radiation squeezing, and optical bistability [30–32]. These nonclassical properties are of growing interest in fundamental spectroscopic investigations and in optical measurement precision [33–35].

By placing a second quantum well inside the cavity, with a judicious choice of the width between the wells, another quasiparticle can be created: the dipolariton. This new hybrid particle is a combination of a polariton and indirect exciton. The first is the result of the coupling between the cavity photonic field and exciton of the left quantum well (called direct exciton), whereas the second is the interaction between a hole of a left and an electron of a right quantum well via electronic tunneling [36]. A powerful feature of the dipolariton cavity is that it constitutes a novel source of generating strong and tunable terahertz radiations [37–40]. Moreover, we have shown in previous works that the system exhibits intriguing optical properties compared to the polariton cavity, and is a good device for producing a strong and thermally resistant squeezing owing to direct and additional indirect excitonic nonlinearities [41–46].

In this paper, we study the photons correlations and the statistical properties of light transmitted by an optical microcavity containing a single, then two, coupled quantum wells and interacting with a Kerr nonlinearity resulting from a third-order nonlinear medium. First, we consider the polariton cavity and we examine the regime of the bistability, the noise spectrum, and the intensity power spectrum. After that, we study the dipolariton cavity in the presence of nonlinearity, and we take the opportunity to compare the two systems. The coupling with thermal environments is considered.

II. POLARITON CAVITY**A. Hamiltonian, quantum dynamics, and fluctuations**

We consider a semiconductor microcavity containing a quantum well placed in a position which corresponds to the maximum of the light field. The cavity has a length of the order of the wavelength λ . On both sides of the microcavity are

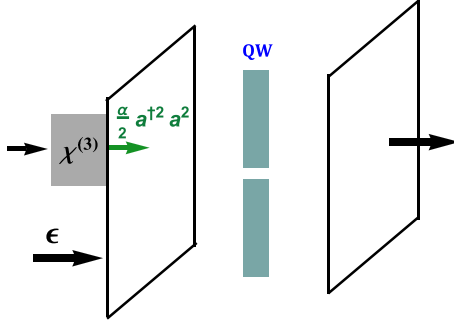


FIG. 1. Schematic diagram of the polariton cavity. The quantum well is placed in the maximum of the electromagnetic field between a set of Bragg mirrors ensuring high reflectivity. The cavity is driven by a coherent field. A Kerr medium is attached to the cavity and the resulting photons from the nonlinear process are directly injected into the cavity.

disposed a set of Bragg mirrors ensuring the high reflectivity of light and allowing us to reach the strong-coupling regime (Fig. 1). The electromagnetic field inside the cavity excites an electron from the filled valence band to the conduction band. As a result, a hole is created in the valence band. The formed electron-hole system possesses bound states called excitonic states, similar to hydrogenic states. Due to the strong coupling of the electromagnetic dipolar oscillations of the excitons and photons, a hybrid light-matter quasiparticle is created: the polariton. Furthermore, we consider a nonlinear $\chi^{(3)}$ medium attached to the cavity in such a way that the produced photons from the nonlinear process interact with the quantum well. The interaction Hamiltonian of the total system including the quantum-well excitons and the $\chi^{(3)}$ medium, in the rotating-wave approximation, is given by ($\hbar = 1$)

$$H = -\delta_a a^\dagger a - \delta_b b^\dagger b + i\epsilon(a^\dagger - a) + i\frac{\Omega}{2}(a^\dagger b + b^\dagger a) + \frac{\alpha}{2}a^\dagger a^\dagger a a. \quad (1)$$

The first term is the energy of the cavity mode where $\delta_a = \omega_l - \omega_c$ is the pump laser-cavity detuning. The second one denotes the free energy of excitons in the quantum well where $\delta_b = \omega_l - \omega_x$ is the frequency detuning between the external pump and the excitonic mode. The interaction of the coherent pump of amplitude ϵ and the cavity mode is described by the third term. The fourth term denotes the interaction between the exciton and the cavity field where Ω characterizes the strength of this coupling. The last term is the Kerr-type photonic nonlinearity with a coefficient α . a^\dagger and b^\dagger are creation operators of the cavity and the excitonic modes, respectively, satisfying the commutation relations given by $[a, a^\dagger] = 1$ and $[b, b^\dagger] = 1$. The quantum Langevin equations describing the time evolution of the two fields are given by

$$\dot{a} = \left(i(\delta_a - \alpha a^\dagger a) - \frac{\kappa}{2}\right)a + \frac{\Omega}{2}b + \epsilon + \sqrt{\kappa}a_{\text{in}}, \quad (2)$$

$$\dot{b} = \left(i\delta_b - \frac{\gamma}{2}\right)b - \frac{\Omega}{2}a + \sqrt{\gamma}b_{\text{in}}, \quad (3)$$

where κ is the decay rate of the cavity mode and γ represents the dissipation rate of the excitonic field. In these equations, $\sqrt{\kappa}a_{\text{in}}$ and $\sqrt{\gamma}b_{\text{in}}$ are the Langevin forces associated with the

reservoirs for the electromagnetic field and for the excitons in the quantum well. The noise correlation functions are obtained from the generalized Einstein relations [47,48] as

$$\langle b_{\text{in}}^\dagger(t)b_{\text{in}}(t') \rangle = n_{\text{th}}\delta(t-t'), \quad (4)$$

$$\langle b_{\text{in}}(t)b_{\text{in}}^\dagger(t') \rangle = (n_{\text{th}} + 1)\delta(t-t'), \quad (5)$$

$$\langle a_{\text{in}}(t)a_{\text{in}}^\dagger(t') \rangle = \delta(t-t'), \quad (6)$$

where n_{th} is the thermal exciton mean number.

B. Photonic intensity and stability analysis

The time dependences of the mean fields are obtained from Eqs. (2) and (3) and governed by the following equations:

$$\dot{\bar{a}} = \left(i(\delta_a - \alpha I_a) - \frac{\kappa}{2}\right)\bar{a} + \frac{\Omega}{2}\bar{b} + \epsilon, \quad (7)$$

$$\dot{\bar{b}} = \left(i\delta_b - \frac{\gamma}{2}\right)\bar{b} - \frac{\Omega}{2}\bar{a}. \quad (8)$$

At the steady state, the previous equations can be solved using the condition $\dot{\bar{a}} = \dot{\bar{b}} = 0$. From the previous set, the steady-state mean number of photons inside the cavity, $I_a = |\bar{a}|^2$, satisfies $I_a[\kappa_0^2 + (-\Delta_{a_0} + \alpha I_a)^2] = |\epsilon|^2$, where

$$\kappa_0 = \frac{\kappa}{2} + \frac{\left(\frac{\Omega}{2}\right)^2 \frac{\gamma}{2}}{\delta_b^2 + \left(\frac{\gamma}{2}\right)^2}, \quad \Delta_{a_0} = \delta_a - \frac{\left(\frac{\Omega}{2}\right)^2 \delta_b}{\delta_b^2 + \left(\frac{\gamma}{2}\right)^2}. \quad (9)$$

To study the bistable behavior, we calculate $\partial|\epsilon|^2/\partial I_a = 0$, which gives the bistability condition as $\Delta_{a_0}^2 - 3\kappa_0^2 > 0$, or explicitly

$$\left[\delta_a^2 - 3\left(\frac{\kappa}{2}\right)^2\right] - 2\beta\left(\delta_a\delta_b + 3\frac{\kappa}{2}\frac{\gamma}{2}\right) + \beta^2\left[\delta_b^2 - 3\left(\frac{\gamma}{2}\right)^2\right] > 0, \quad (10)$$

where β is given by $\beta = \left(\frac{\Omega}{2}\right)^2/[\delta_b^2 + \left(\frac{\gamma}{2}\right)^2]$. In the absence of a quantum well ($\beta = 0$), the bistability condition reduces simply to $\delta_a^2 > 3\left(\frac{\kappa}{2}\right)^2$. Moreover, the solution for I_a should be real and positive. With these conditions, the bistability is obtained when $\delta_a < -\sqrt{3}\kappa/2$, i.e., $\omega_c > \sqrt{3}\kappa/2 + \omega_l$. This corresponds to the condition of a Kerr medium, without additional couplings.

It is useful to normalize the parameters of the system to the round-trip time of photons inside the cavity τ_c . In our study, the numerical values of the system parameters are chosen in such a way that they are close to that of a typical experiment [45,49–53].

Figure 2 represents the intracavity photonic intensity in two coupling regimes as a function of the frequency detuning for various nonlinearity coefficients α (after assuming that $\delta_a = \delta_b = \Delta$ and $\kappa = 2\gamma$). For strong coupling ($\Omega \gg \gamma, \kappa$), the intensity is centered around the detunings $\Delta = \pm\Omega/2$ in the case of zero or weak nonlinearities. As the interaction between the photons increases, the intensity peaks are blueshifted and decrease progressively. However, in the weak-coupling regime ($\Omega \ll \gamma, \kappa$) the intensity peak is around the resonance but also decreases with the nonlinearity. We note here that the maximum of intensity in weak coupling is stronger than that of strong coupling. Furthermore, we conclude that the

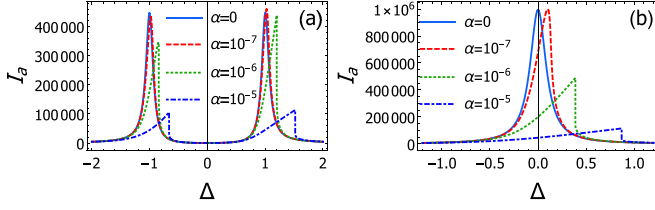


FIG. 2. Photonic intensities in (a) the strong-coupling regime ($\Omega = 2, \gamma = 0.05, \epsilon = 100$, and $\kappa = 0.1$), and (b) for the weak coupling ($\Omega = 0.008, \gamma = 0.05, \epsilon = 100$, and $\kappa = 0.1$) as a function of the detuning for various nonlinearity coefficients α .

nonlinear interaction between photons is unfavorable to strong photonic intensity and creates a dissymmetry of the peaks.

In Fig. 3, we plot the photonic intensity as a function of the laser pumping amplitude for various dissipation rates. The increase of the input field is favorable to higher intensity inside the cavity for weaker decay rates. The system is fully stable. The bistability behavior can be controlled by varying the power of the laser field and the detunings. By choosing appropriate values that satisfy Eq. (10), the bistability is represented by Fig. 3(b) as a function of the square of ϵ which is proportional to the power of the coherent pump. This clearly shows a parameter region for which the dynamics of the system becomes unstable. By increasing the external pump power, the system reaches the first bistable point. Then, the hysteresis follows the narrow and jumps to the upper branch. To obtain the second bistable point, we should scan the input power for lower values.

C. Fluctuation spectrum

Now, we analyze the noise properties of the light transmitted by the polariton cavity. The operators of the system can be split into the mean value of the field and its fluctuation term as $a = \bar{a} + \delta a$ and $b = \bar{b} + \delta b$. The fluctuation operators δa and δb satisfy the following relations: $[\delta a, \delta a^\dagger] = 1$ and $[\delta b, \delta b^\dagger] = 1$. They are very small compared to their corresponding mean values. Thus, using Eqs. (2) and (3) and

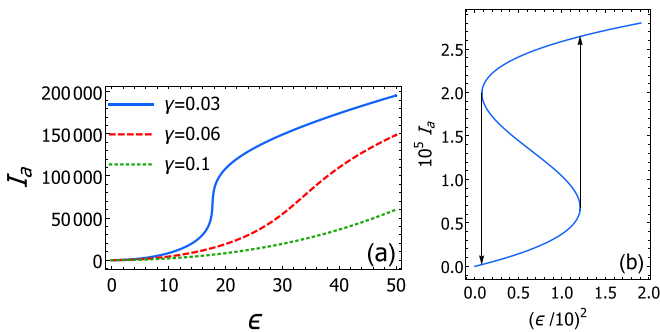


FIG. 3. (a) Photonic intensity as a function of the coherent pump amplitude ϵ for various dissipation rates ($\Omega = 0.008, \alpha = 10^{-6}$, and $\Delta = 0.1$). (b) Photonic intensity as a function of the square of the coherent pump amplitude ϵ for $\Omega = 0.008, \alpha = 10^{-6}, \Delta = 0.2, \gamma = 0.02$, and $\kappa = 0.04$: optical bistability.

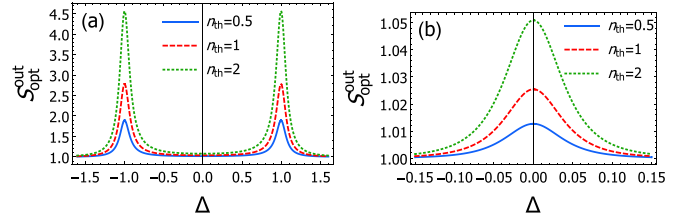


FIG. 4. Variation of the noise spectrum vs the frequency detuning for various bath temperature values for (a) strong coupling ($\alpha = 0, \Omega = 2, \gamma = 0.05, \kappa = 0.1$, and $\epsilon = 100$) and (b) weak coupling ($\alpha = 0, \Omega = 0.008, \gamma = 0.05, \kappa = 0.1$, and $\epsilon = 100$).

Eqs. (7) and (8), we obtain the following linearized evolution equations for the fluctuations:

$$\delta \dot{a} = \left(i(\delta_a - 2\alpha I_a) - \frac{\kappa}{2} \right) \delta a - i\alpha \bar{a}^2 \delta a^\dagger + \frac{\Omega}{2} \delta b + \sqrt{\kappa} a_{\text{in}}, \quad (11)$$

$$\delta \dot{b} = \left(i\delta_b - \frac{\gamma}{2} \right) \delta b - \frac{\Omega}{2} \delta a + \sqrt{\gamma} b_{\text{in}}. \quad (12)$$

The fluctuation spectrum of the single-mode cavity is defined as the Fourier transform of the two-time correlation $\langle \delta X_\theta(t + \tau) \delta X_\theta(t) \rangle_{ss}$ [54],

$$S_\theta(\omega) = \int_{-\infty}^{+\infty} \langle \delta X_\theta(t + \tau) \delta X_\theta(t) \rangle_{ss} e^{-i(\omega - \omega_0)\tau} d\tau \\ = \langle \delta X_\theta(\omega) \delta X_\theta(\omega) \rangle, \quad (13)$$

where $\delta X_\theta(\omega) = e^{-i\theta} \delta a(\omega) + e^{i\theta} \delta a^\dagger(\omega)$ is a field quadrature and θ represents its controllable phase. A light has the property of nonclassicality, or squeezing, if one of its quadratures has fluctuations where one of the frequency components shows lower noise than the standard quantum noise, that is to say, $[S_\theta(\omega)]_{\text{shot}} = 1$. In other words, if it exists, θ and ω satisfy $S_\theta(\omega) < 1$. Equation (13) takes the form

$$S_\theta(\omega) = C_{aa}(\omega) e^{-2i\theta} + C_{a^\dagger a^\dagger}(\omega) e^{2i\theta} \\ + C_{a^\dagger a}(\omega) + C_{aa^\dagger}(\omega), \quad (14)$$

where $C_{aa}, C_{a^\dagger a^\dagger}, C_{a^\dagger a}$, and C_{aa^\dagger} are the correlation functions of the intracavity field fluctuations defined by $\langle \delta o_1(\omega) \delta o_2(\omega') \rangle = 2\pi \delta(\omega + \omega') C_{o_1 o_2}(\omega)$, $(o_1, o_2) \in \{a, a^\dagger\}$. The optimum fluctuation spectrum is defined by $S_{\text{opt}}(\omega) = \min_{\theta \in [0, 2\pi]}$. The correspondent quadrature is obtained by minimizing Eq. (14) with respect to the phase angle θ [$dS_\theta(\omega)/d\theta = 0$]. The optimal angle θ_{opt} then satisfies $e^{2i\theta_{\text{opt}}} = -C_{aa}(\omega)/|C_{aa}(\omega)|$. Combining the previous equations, we obtain the following relation of the optimized fluctuation spectrum: $S_{\text{opt}}(\omega) = -2|C_{aa}(\omega)| + C_{aa^\dagger}(\omega) + C_{a^\dagger a}(\omega)$. For our system, these correlation functions can be derived by solving Eqs. (11) and (12) in Fourier space which yields for the fluctuating photonic field a linear combination of the noise operators as $\delta a(\omega) = \sqrt{\kappa} \zeta_1(\omega) a_{\text{in}}(\omega) + \sqrt{\gamma} \zeta_2(\omega) b_{\text{in}}(\omega) + \sqrt{\kappa} \zeta_3(\omega) a_{\text{in}}^\dagger(\omega) + \sqrt{\gamma} \zeta_4(\omega) b_{\text{in}}^\dagger(\omega)$.

The standard input-output relation $\delta a^{\text{out}} = \sqrt{\kappa} \delta a - a^{\text{in}}$ and its Hermitian conjugated $\delta a^{\dagger \text{out}} = \sqrt{\kappa} \delta a^\dagger - a^{\text{in} \dagger}$ allow us to obtain the correlations in the output of the cavity. With the help of these relations, we can express the fluctuation

spectrum of the emergent light as

$$S_{\text{opt}}^{\text{out}} = 1 - 2\kappa |\kappa \zeta_1(\omega) \zeta_3(-\omega) + \gamma(n_{\text{th}} + 1) \zeta_2(\omega) \zeta_4(-\omega) - \zeta_3(-\omega)| + \kappa(\kappa |\zeta_1(\omega)|^2 + \gamma(n_{\text{th}} + 1) |\zeta_2(\omega)|^2 + \gamma n_{\text{th}} |\zeta_4(\omega)|^2 - 2 \text{Re}[\zeta_1(\omega)]) + \kappa(\kappa |\zeta_3(-\omega)|^2 + \gamma n_{\text{th}} |\zeta_2(-\omega)| + \gamma(n_{\text{th}} + 1) |\zeta_4(-\omega)|^2), \quad (15)$$

where ζ_i are functions of the system parameters. $S_{\text{opt}}^{\text{out}} = 1$ corresponds to the standard quantum noise, whereas when $S_{\text{opt}}^{\text{out}} > 1$ the transmitted light shows fluctuations above the standard limit. $S_{\text{opt}}^{\text{out}} < 1$ is a signature of nonclassical properties of light, the squeezing effect.

D. Spectrum of the linear system

When the nonlinear interaction between photons is not strong enough, the term $(\alpha a^\dagger a^\dagger a a / 2)$ can be neglected compared to the other terms of the Hamiltonian (1). In this linear system case, the transmitted field cannot exhibit fluctuations below the vacuum level, and consequently is unable to show the squeezing effect. Moreover, as the bath temperature increases, the fluctuations are above the vacuum level and appear around the detunings $\Delta = \pm \Omega/2$ in the strong-coupling regime [Fig. 4(a)]. In the weak-coupling regime [Fig. 4(b)], we observe small fluctuations localized around the resonance weakly dependent on the temperature. Away from these particular detunings, the emitted light is coherent.

E. Squeezing of the output field

In the case where the photonic nonlinearity is important, the nonlinear term in the Hamiltonian must be considered. This interaction gives rise to fluctuations under the standard quantum noise or the squeezing effect. This nonclassical effect occurs for specific frequency detunings equal to half of the constant coupling Ω , when the strong-coupling regime is reached [Fig. 5(a)]. For increasing nonlinearities, a stronger squeezing is realized and the squeezing peaks lose their symmetry progressively. In the weak-coupling regime [Fig. 5(b)] and for weak values of α , the nonclassical effect is centered around the resonance. An increase of nonlinearity generates higher squeezing and also a dissymmetry. We notice here that the weak coupling is more favorable to higher squeezing than the strong coupling. Figure 5(c) depicts the variation of the squeezing as a function of the detuning and the coupling constant Ω for a fixed value of nonlinearity. It is shown that in the weak-coupling regime ($\Omega \ll \kappa, \gamma$), the nonclassical effect is at its maximum. As the photon-exciton interaction increases, the emitted light becomes less squeezed and the spectrum is duplicated into two branches following a *V form*.

We have to mention here the peaks of the noise spectrum are blueshifted and follow the behavior of the photonic intensity (Fig. 2). This effect can be explained by the fact that the strong light-matter coupling in the system (exciton-photon coupling) induces a generation of two polaritonic branches: the upper polaritonic branch and the lower polaritonic branch. The nonlinearity favors one branch over the other: the lower polaritonic branch [31,55].

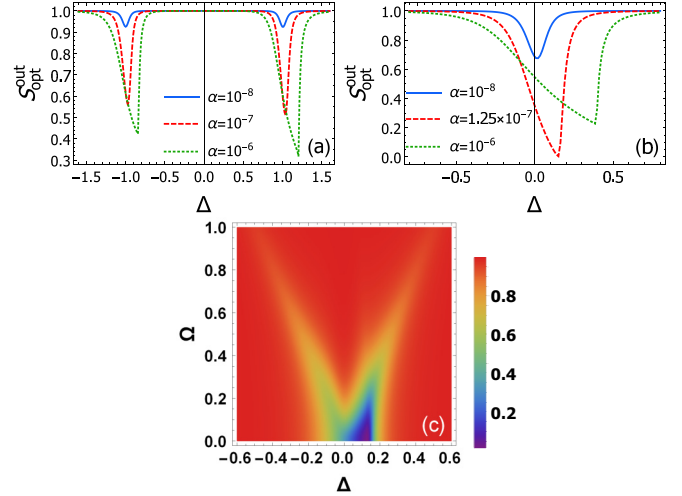


FIG. 5. The zero-temperature dependence of the noise spectrum on the frequency detuning for various nonlinearity coefficients α (a) in the strong-coupling regime ($\Omega = 2$) and (b) in the weak-coupling regime ($\Omega = 0.008$). (c) Density plot of the noise spectrum as a function of the detuning and the coupling constant Ω for $\alpha = 10^{-7}$. In all plots, the other parameters are chosen to be $\gamma = 0.05$, $\epsilon = 100$, and $\kappa = 0.1$.

F. Squeezing and temperature

Here, we discuss the stability of the nonclassical effect produced by photonic nonlinearity. In Fig. 6(a) we plot the variation of the noise spectrum in the strong-coupling regime as a function of the nonlinearity coefficient α at zero temperature ($T = 0$). First, for weak nonlinearities, the squeezing increases with increasing α and reaches a maximum approaching 70%. After that, it decreases progressively towards the coherent light ($S_{\text{opt}}^{\text{out}} = 1$). For a nonzero bath temperature ($n_{\text{th}} = 0.2$), the maximum squeezing of the previous situation is rapidly transformed to high fluctuations, and the whole system loses some amount of squeezing [Fig. 6(b)]. In the

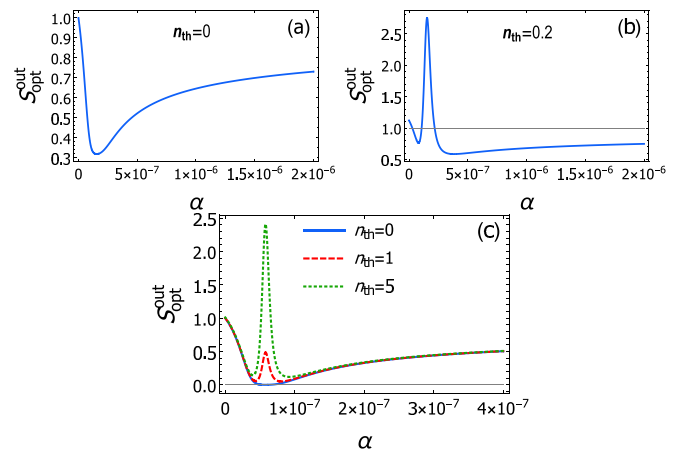


FIG. 6. Variation of the noise spectrum of the polariton cavity as a function of the photonic nonlinearity α and the temperature of the thermal bath in the (a), (b) strong-coupling regime ($\Omega = 2$, $\gamma = 0.05$, $\Delta = 1.05$, $\epsilon = 100$, and $\kappa = 0.1$) and (c) for weak coupling ($\Omega = 0.008$, $\gamma = 0.05$, $\Delta = 0.08$, $\epsilon = 100$, and $\kappa = 0.1$).

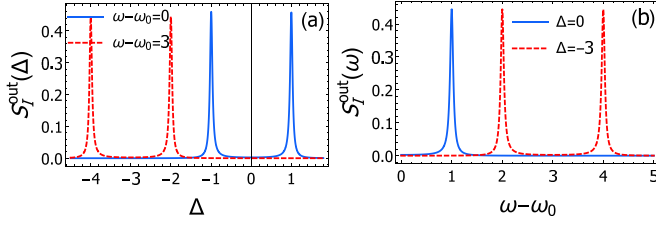


FIG. 7. Intensity power spectrum of the output field in the strong-coupling regime as a function of (a) the detuning and (b) the frequency for $\alpha = 10^{-8}$, $\Omega = 2$, $\gamma = 0.05$, $\kappa = 0.1$, $\epsilon = 100$, and $n_{th} = 0.5$.

weak-coupling regime [Fig. 6(c)], the emitted light may be perfectly squeezed for a weak range of α . With increasing temperature, this range of maximum squeezing shows strong fluctuations above the vacuum level, whereas this spectrum is still unchanged for the other nonlinearities. Moreover, we notice a higher resistance against the bath temperature than the strong-coupling regime.

In conclusion, it is clear that the temperature destroys the nonclassical effect in the strong-coupling regime. However, in the weak-coupling regime it is weakly affected except for a small range of α .

G. Intensity power spectrum

The intensity power spectrum of the transmitted radiation is defined as the Fourier transform of the correlation $\langle \delta a^{\dagger out}(t + \tau) \delta a^{out}(t) \rangle$:

$$S_I^{out}(\omega) = \int_{-\infty}^{+\infty} d\tau e^{-i(\omega - \omega_0)\tau} \langle \delta a^{\dagger out}(t + \tau) \delta a^{out}(t) \rangle = C_{a^\dagger a}^{out}(\omega) = \kappa C_{a^\dagger a}(\omega). \quad (16)$$

In Fig. 7(a) we plot the intensity power spectrum outside the cavity as a function of the detuning. At zero frequency ($\omega - \omega_0 = 0$), the spectrum is formed by two peaks of maximal intensity centered around the coupling constants $\pm\Omega/2$ and then separated by Ω . For higher frequency ($\omega - \omega_0 = 3$), the spectrum is translated to negative detunings. However, the peaks keep the same intensities, and also the same spacing. The variation against the frequency is illustrated by Fig. 7(b). At the resonance the spectrum consists of a single peak around $\omega - \omega_0 = \Omega/2$. By increasing the detuning, the peak is duplicated and the whole spectrum is centered around $\omega - \omega_0 = |\Delta|$.

III. DIPOLARITON CAVITY

A. Hamiltonian, quantum dynamics, and fluctuations

In this section, we consider the dipolariton cavity. This system is formed by two coupled quantum wells in a semiconductor microcavity, confined between a set of Bragg mirrors with high reflection (Fig. 8). Because the quantum wells are with different band gaps, the cavity mode excites only electrons of the first quantum well and forms a direct exciton. Via an electronic tunneling, a second quasiparticle appears as a result of the interaction between holes appertaining to the first quantum well and electrons localized in the second quantum

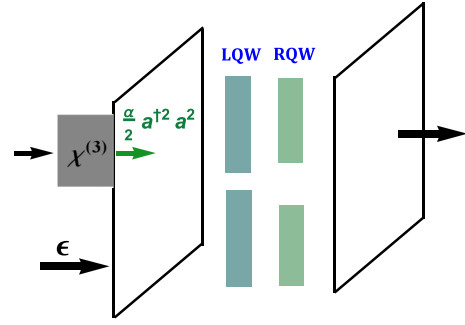


FIG. 8. Schematic diagram of the dipolariton cavity. The two quantum wells are placed between a highly reflecting set of Bragg mirrors. The wells are coupled via a tunnel effect with a tunneling rate J . The cavity is driven by a coherent field. A Kerr medium is attached to the cavity and the resulting photons from the nonlinear process are directly injected into the cavity.

well: an indirect exciton. This tunnel effect is allowed owing to the thin barrier separating the wells. When the electron levels of both quantum wells are tuned into resonance, a strong coupling is achieved between the direct and indirect excitons. As a consequence, the whole system shows three eigenmodes: a lower dipolariton, middle dipolariton, and an upper dipolariton. The interaction of the nonlinear medium with the cavity is the same as for the polariton cavity discussed above. The total system Hamiltonian can be written as ($\hbar = 1$)

$$H = -\delta_a a^\dagger a - \delta_b b^\dagger b - \delta_c c^\dagger c + i\epsilon(a^\dagger - a) + i\frac{\Omega}{2}(a^\dagger b - b^\dagger a) + i\frac{J}{2}(b^\dagger c - c^\dagger b) + \frac{\alpha}{2} a^\dagger a^\dagger a a, \quad (17)$$

where b now denotes the annihilation operator of the direct exciton and c is the annihilation operator of the indirect excitonic mode. The parameter J characterizes the rate of tunneling between the coupled wells, and thus indicates the coupling strength between direct and indirect excitons. $\delta_c = \omega_l - \omega_{ix}$ is the frequency detuning between the coherent pump frequency and the indirect excitonic mode. The quantum Langevin equations of the three modes of the system are expressed as

$$\dot{a} = \left(i(\delta_a - \alpha a^\dagger a) - \frac{\kappa}{2} \right) a + \frac{\Omega}{2} b + \epsilon + \sqrt{\kappa} a_{in}, \quad (18)$$

$$\dot{b} = \left(i\delta_b - \frac{\gamma_b}{2} \right) b - \frac{\Omega}{2} a + \frac{J}{2} c + \sqrt{\gamma_b} b_{in}, \quad (19)$$

$$\dot{c} = \left(i\delta_c - \frac{\gamma_c}{2} \right) c - \frac{J}{2} b + \sqrt{\gamma_c} c_{in}. \quad (20)$$

$a_{in}(t)$, $b_{in}(t)$, and $c_{in}(t)$ are the Langevin noise operators of the cavity and the excitonic modes. γ_c denotes the damping rate of the indirect exciton mode. As thermal excitations in the excitonic fields are not necessarily the same, then the noise operators satisfy the following equations,

$$\langle b_{in}^\dagger(t) b_{in}(t') \rangle = n_{dx} \delta(t - t'), \quad (21)$$

$$\langle b_{in}(t) b_{in}^\dagger(t') \rangle = (n_{dx} + 1) \delta(t - t'), \quad (22)$$

$$\langle c_{in}^\dagger(t) c_{in}(t') \rangle = n_{ix} \delta(t - t'), \quad (23)$$

$$\langle c_{in}(t) c_{in}^\dagger(t') \rangle = (n_{ix} + 1) \delta(t - t'), \quad (24)$$

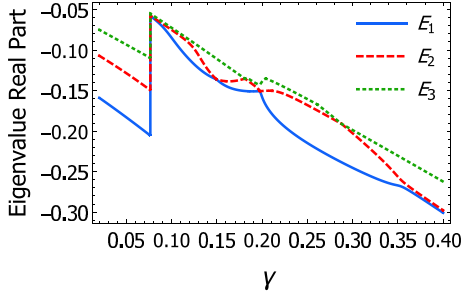


FIG. 9. The real parts of the system eigenvalues represented as a function of the decay rate γ for $\epsilon = 100$, $\Omega = J = 2$, $\alpha = 10^{-6}$, and $\Delta = 0.1$.

where n_{dx} and n_{ix} are the direct and indirect thermal excitons mean numbers, respectively.

B. Validity of the steady-state solutions

In the following sections, the performed study is based on the steady-state solutions of the Langevin equations. However, it is not obvious that this system always reaches a steady state. For some parameter regimes, in particular in the strong-coupling regime, the system could also end up in some oscillatory behavior in density between direct and indirect excitonic modes, never reaching a steady state [37]. Here, we make sure of the validity of the steady-state regime. Our system is an open quantum system (coupled to an environment). In the quantum Markovian description, the environment is modeled as a thermal reservoir with a short correlation time and weakly coupled to the system. This kind of system is described by a non-Hermitian Hamiltonian H with complex eigenvalues $\mathcal{E}_k = E_k + \frac{i}{2}\Gamma_k$. These eigenvalues provide the energies E_k of the states and their lifetimes defined by the inverse of the widths Γ_k [56,57]. The set of equations (18)–(20) has the form $dU/dt = LU + F$. Mathematically, if the matrix L has all eigenvalues so that the real part of each eigenvalue is negative, then the stability of the system is assured and we will not have oscillatory stationary values. All the parameters used in our study fulfill this condition with respect to the dissipation rates. As we can observe in Fig. 9, all the real parts of the eigenvalues E_k of the system are negative.

C. Photonic intensity and stability analysis

The time evolutions of the mean fields are deduced from the set (18)–(20) and read

$$\dot{\bar{a}} = \left(i(\delta_a - \alpha I_a) - \frac{\kappa}{2} \right) \bar{a} + \frac{\Omega}{2} \bar{b} + \epsilon, \quad (25)$$

$$\dot{\bar{b}} = \left(i\delta_b - \frac{\gamma_b}{2} \right) \bar{b} - \frac{\Omega}{2} \bar{a} + \frac{J}{2} \bar{c}, \quad (26)$$

$$\dot{\bar{c}} = \left(i\delta_c - \frac{\gamma_c}{2} \right) \bar{c} - \frac{J}{2} \bar{b}. \quad (27)$$

The solution with respect to the photonic mean field in the steady state yields

$$\bar{a} = \frac{\epsilon}{\kappa'_0 + i(-\Delta'_{a0} + \alpha I_a)}, \quad (28)$$

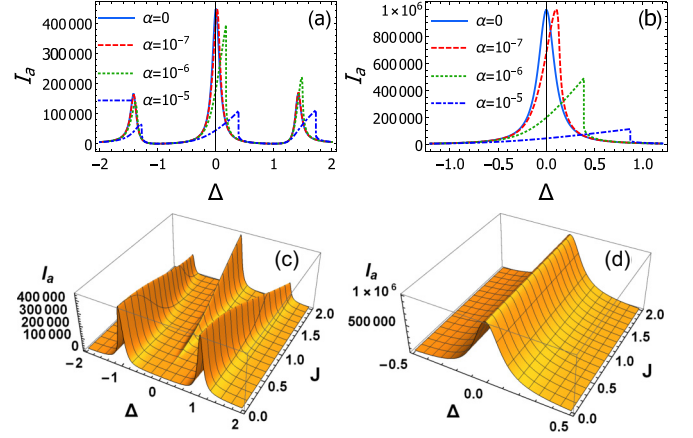


FIG. 10. Photonic intensity in (a) the strong-coupling regime vs the detuning for $\Omega = J = 2$, $\gamma = 0.05$, and $\kappa = 0.1$, and for (b) the weak coupling vs the detuning for $\Omega = J = 0.008$, $\gamma = 0.05$, and $\kappa = 0.1$. Both representations are calculated for several nonlinearity coefficients. (c) and (d) are three-dimensional (3D) plots of the photonic intensities vs the tunneling rate J and the detuning in the strong- and weak-coupling regimes, respectively, for $\alpha = 10^{-8}$ [the other parameters are the same as (a) and (b)].

where

$$\kappa'_0 = \frac{\kappa}{2} + \frac{(\frac{\Omega}{2})^2 (\frac{\gamma_b}{2} + \frac{\gamma_c}{2} \beta_c)}{(\frac{\gamma_b}{2} + \frac{\gamma_c}{2} \beta_c)^2 + (\delta_b - \beta_c \delta_c)^2}, \quad (29)$$

$$\Delta'_{a0} = \delta_a - \frac{(\frac{\Omega}{2})^2 (\delta_b - \delta_c \beta_c)}{(\frac{\gamma_b}{2} + \frac{\gamma_c}{2} \beta_c)^2 + (\delta_b - \beta_c \delta_c)^2}, \quad (30)$$

and β_c is given by $\beta_c = (J/2)^2 / [\delta_c^2 + (\frac{\gamma_c}{2})^2]$ which contains the indirect exciton parameters. Similarly to the calculation made above for the polariton cavity, from Eq. (28) we get for the photonic intensity $I_a [\kappa'_0 + (-\Delta'_{a0} + \alpha I_a)^2] = |\epsilon|^2$. Furthermore, the intracavity direct and indirect excitonic intensities are linked by $I_c = \beta_c I_b$, and we have

$$I_b = \frac{(\frac{\Omega}{2})^2}{(\frac{\gamma_b}{2} + \frac{\gamma_c}{2} \beta_c)^2 + (\delta_b - \beta_c \delta_c)^2} I_a. \quad (31)$$

The bistability condition $\Delta_{a0}^2 - 3\kappa_0^2 > 0$ yields in this case

$$\left[\delta_a^2 - 3 \left(\frac{\kappa}{2} \right)^2 \right] - 2\beta_{b,c} \left[\delta_a (\delta_b - \delta_c \beta_c) + 3 \frac{\kappa}{2} \left(\frac{\gamma_b}{2} + \frac{\gamma_c}{2} \beta_c \right) \right] + \beta_{b,c}^2 \left[(\delta_b - \delta_c \beta_c)^2 - 3 \left(\frac{\gamma_b}{2} + \frac{\gamma_c}{2} \beta_c \right)^2 \right] > 0, \quad (32)$$

where the quantity $\beta_{b,c}$ is given by

$$\beta_{b,c} = \frac{(\frac{\Omega}{2})^2}{(\frac{\gamma_b}{2} + \frac{\gamma_c}{2} \beta_c)^2 + (\delta_b - \beta_c \delta_c)^2}, \quad (33)$$

taking into account the direct and indirect exciton parameters. It is clear that in the absence of the second quantum well ($\beta_c = 0$), Eq. (32) reduces to the same bistability condition given by Eq. (10) for the polariton cavity.

Differently from the polariton cavity, the photonic intensity of the linear dipolariton system in the strong-coupling regime [Fig. 10(a)] shows three peaks: a big peak at resonance and two small symmetrical peaks centered around the particular

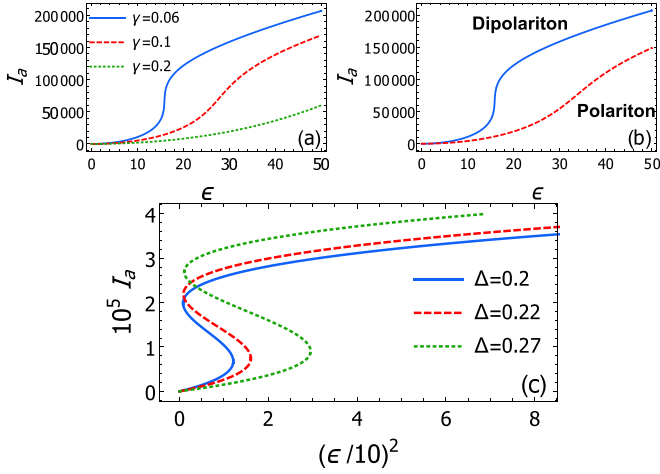


FIG. 11. (a) Photonic intensity as a function of the coherent pump amplitude ϵ for various damping rates ($\Omega = 0.008$, $\alpha = 10^{-6}$, $\Delta = 0.1$, and $\epsilon = 100$). (b) Comparison of the photonic intensities between the polariton and the dipolariton cavity before the regime of the optical bistability for $\gamma = 0.06$. The other parameters are the same as (a). (c) Photonic intensity as a function of the square of the coherent pump amplitude ϵ for $\Omega = 0.008$, $\alpha = 10^{-6}$, $\gamma = 0.02$, $\kappa = 0.04$, and three detunings Δ : optical bistability.

detunings $\pm\Omega/\sqrt{2}$. As the nonlinearity increases, the intensity peaks are blueshifted and decrease considerably for sufficiently strong values of α . For weak coupling [Fig. 10(b)], the photonic intensity is localized around the resonance and is stronger than that of the strong coupling. The tunneling between the wells is an additional important parameter. It describes the degree of the interaction between the wells, and thus the strength of the coupling between direct and indirect excitons. The variation of the intensity versus the tunneling rate J is illustrated by Figs. 10(c) and 10(d). We clearly observe that in the strong-coupling regime and in the absence of the tunneling, the photonic intensity is similar to that of the polariton system. When the tunneling becomes important, a third peak appears at resonance and reaches its maximum for $\Omega = J$. In return, the symmetrical peaks decrease correspondingly. In the weak-coupling regime, the intensity is quasi-independent on the tunneling rate. Consequently, the polariton and dipolariton cavities are similar in this regime.

By varying the amplitude of the coherent pump field, we plot the dependence of I_a against ϵ before the regime of the bistability [Fig. 11(a)]. The intensity increases with decreasing direct and indirect excitonic damping rates. As a comparison of the two systems and by choosing the same physical parameters, we conclude that the dipolariton cavity reaches the regime of the optical bistability before the polariton cavity [Fig. 11(b)]. When the condition (32) is fulfilled, the bistable behavior appears [Fig. 11(c)]. This indicates that the dynamics of the system exhibit an instability in a certain parameter region.

D. Fluctuation spectrum

In order to determine the expression of the fluctuation spectrum, the system operators are decomposed into two parts: a

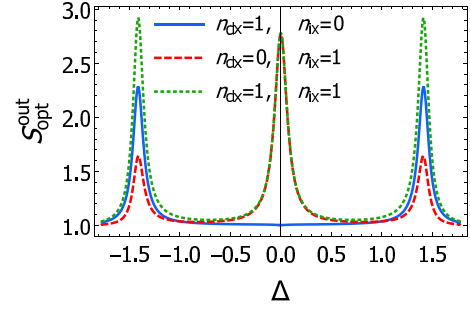


FIG. 12. Variation of the spectrum of noise as a function of the frequency detuning for various bath temperature values in the strong-coupling regime. The parameters are $\alpha = 0$, $\Omega = J = 2$, $\gamma = 0.05$, $\epsilon = 100$, and $\kappa = 0.1$.

mean field and fluctuation such as $a = \bar{a} + \delta a$, $b = \bar{b} + \delta b$, and $c = \bar{c} + \delta c$. Adopting the same procedure as for the polariton cavity, we get the following set of linearized evolution equations of the fluctuations:

$$\delta\dot{a} = \left(i(\delta_a - 2\alpha I_a) - \frac{\kappa}{2} \right) \delta a - i\alpha \bar{a}^2 \delta a^\dagger + \frac{\Omega}{2} \delta b + \sqrt{\kappa} a_{\text{in}}, \quad (34)$$

$$\delta\dot{b} = \left(i\delta_b - \frac{\gamma_b}{2} \right) \delta b - \frac{\Omega}{2} \delta a + \frac{J}{2} \delta c + \sqrt{\gamma_b} b_{\text{in}}, \quad (35)$$

$$\delta\dot{c} = \left(i\delta_c - \frac{\gamma_c}{2} \right) \delta c - \frac{J}{2} \delta b + \sqrt{\gamma_c} c_{\text{in}}. \quad (36)$$

In this case, the solution of such a system for the fluctuating cavity field $\delta a(\omega)$ is in the form $\delta a(\omega) = \sqrt{\kappa} \eta_1(\omega) a_{\text{in}} + \sqrt{\gamma_b} \eta_2(\omega) b_{\text{in}} + \sqrt{\gamma_c} \eta_3(\omega) c_{\text{in}} + \sqrt{\kappa} \eta_4(\omega) a_{\text{in}}^\dagger + \sqrt{\gamma_b} \eta_5(\omega) b_{\text{in}}^\dagger + \sqrt{\gamma_c} \eta_6(\omega) c_{\text{in}}^\dagger$. Then, the output optimum noise spectrum is written as

$$\begin{aligned} S_{\text{opt}}^{\text{out}} = & 1 - 2\kappa [|\kappa \eta_1(\omega) \eta_4(-\omega) + \gamma_b (n_{dx} + 1) \eta_2(\omega) \eta_5(-\omega) \\ & + \gamma_c (n_{ix} + 1) \eta_3(\omega) \eta_6(-\omega) - \eta_4(-\omega)|] \\ & + \kappa (\kappa |\eta_1(\omega)|^2 + \gamma_b (n_{dx} + 1) |\eta_2(\omega)|^2 \\ & + \gamma_b n_{dx} |\eta_5(\omega)|^2 + \gamma_c (n_{ix} + 1) |\eta_3(\omega)|^2) \\ & + \kappa (\kappa |\eta_4(-\omega)|^2 + \gamma_b n_{dx} |\eta_2(-\omega)|^2 \\ & + \gamma_b (n_{dx} + 1) |\eta_5(-\omega)|^2 + \gamma_c n_{ix} |\eta_3(-\omega)|^2) \\ & + \kappa \gamma_c n_{ix} |\eta_6(\omega)|^2 + \kappa \gamma_c (n_{ix} + 1) |\eta_6(-\omega)|^2 \\ & - 2\kappa \text{Re}[\eta_1(\omega)]. \end{aligned} \quad (37)$$

E. Spectrum of the linear system

First, we consider the linear system. As shown in Fig. 12, when thermal excitations occur only in the direct excitonic field (solid line), the spectrum shows two symmetrical peaks around $\Delta = \pm\Omega/\sqrt{2}$. When indirect thermal excitons come into play (dashed and dotted lines), first we observe three peaks where the biggest is at resonance, then the two symmetrical peaks gain more fluctuations. In the weak-coupling regime, we obtain similar curves than as for the polariton cavity (figure is not shown here). In conclusion, the degree of the fluctuations depends on the strength of the coupling. Furthermore, the dipolariton system generates higher fluctu-

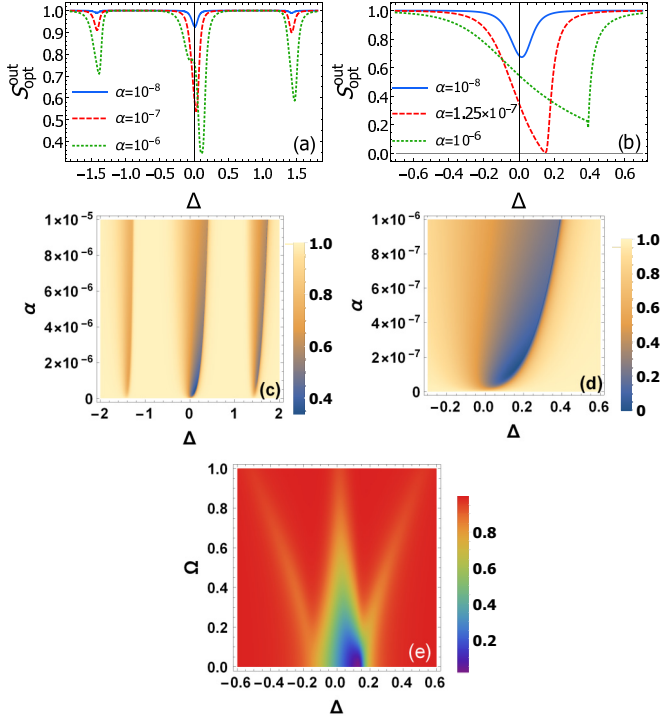


FIG. 13. Squeezing spectrum as a function of the detuning and the nonlinearity coefficient for some values of α [(a), (b)], and a continuous variation of α [(c), (d)]. (a) and (c) represent the strong-coupling regime for $\Omega = J = 2$. (b) and (d) represent the weak-coupling regime for $\Omega = J = 0.008$. (e) Density plot of the noise spectrum as a function of the detuning and the coupling constant Ω for $J = 0.3$ and $\alpha = 10^{-7}$. In all representations, $\gamma = 0.05$, $\epsilon = 100$, and $\kappa = 0.1$.

ations than the polariton cavity. These additional fluctuations appear essentially at resonance.

F. Squeezing of the output field

Now we turn our attention to the squeezing generated by the nonlinear photonic term. It is shown in Fig. 13(a) that in the strong-coupling regime the spectrum is formed by three squeezed peaks. The maximal squeezing is obtained at resonance and the two other peaks are centered around $\Delta = \pm\Omega/\sqrt{2}$. By increasing the nonlinearity coefficient from 10^{-8} to 10^{-6} in normalized units, the squeezing is strongly enhanced with a slight dissymmetry towards the positive detunings. We notice the same behavior in the weak-coupling regime [Fig. 13(b)] except that the nonclassical effect appears only around the resonance and may be perfect with a judicious choice of detuning. This entirely squeezed radiation was already expected in nonlinear quantum systems [58,59]. For an in-depth overview of the situation, we vary the nonlinearity coefficient continuously in both regimes. For strong coupling, we observe three squeezed branches with a small blueshift compared to the initial position of detunings [Fig. 13(c)]. In the weak-coupling regime [Fig. 13(d)], a perfect squeezing is attainable for some region of nonlinearity and increasing frequency detunings. The variation with respect to the photon-exciton coupling strength Ω is illustrated by Fig. 13(e). We

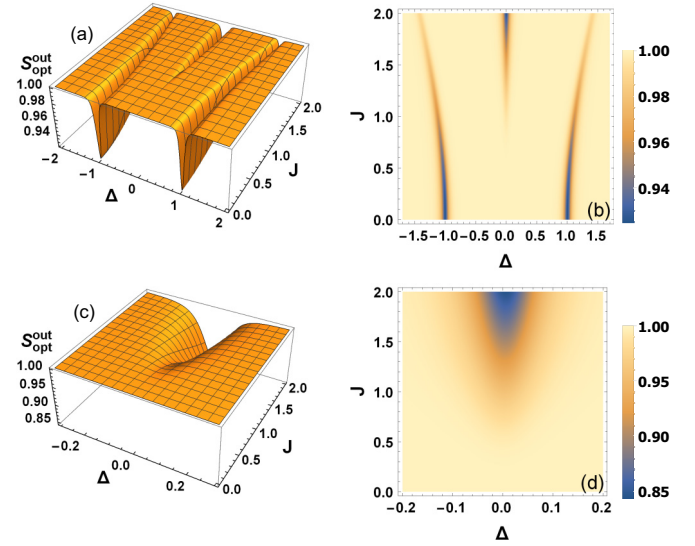


FIG. 14. 3D and density plots of the squeezing spectrum vs the tunneling rate J in the strong-coupling regime [(a), (b)] for $\Omega = 2$, and for the weak coupling [(c), (d)] for $\Omega = 0.008$. In all representations, the other parameters are $\gamma = 0.05$, $\kappa = 0.1$, and $\alpha = 10^{-8}$.

observe, as for the polariton cavity, that the squeezing is maximal for weak coupling. However, as soon as the interaction becomes important ($\Omega \gg \kappa, \gamma$), the spectrum shows three branches of squeezing in *W form* with a decrease of the magnitude of the nonclassical effect.

It is worth noting that, similarly to the polariton cavity case, the forms of the noise spectrum and the blueshift character are imposed by the photonic intensity. The system favors also a dipolaritonic branch over the two others.

G. Squeezing and electronic tunneling

The electronic tunneling between the quantum wells is an important factor as it decides the nature of the created quasi-particles in the cavity, and governs the passage of the system from the polaritonic to dipolaritonic cavity. The magnitude of this effect is imposed by the barrier width which separates the quantum wells. From this, two regimes are observed: a pulsed tunneling if $\Omega > J$ and a pulsed lasing when $J > \Omega$. Experimentally, the first regime corresponds to a barrier width L_B greater than 4 nm, however, the pulsed lasing occurs if $L_B < 4$ nm [36]. We consider first the regime of strong coupling. The 3D and density plots of Figs. 14(a) and 14(b) show that the fluctuation spectrum consists of three branches of squeezed states in the emergent light. Except in these branches, the light is coherently transmitted ($S_{\text{opt}}^{\text{out}} = 1$). We also observe that for $J = 0$ ($L_B > 15$ nm), the quantum wells are decoupled. This seems evident because by increasing the distance between them, the tunneling will not happen and the indirect excitons cannot be created. In this situation, the system is equivalent to the polariton cavity showing two peaks centered around the detunings $\Delta = \pm\Omega/2$. If one decreases the widths, and thus increasing the tunneling, a third branch appears at resonance. Meanwhile, the symmetrical branches deviate from the initial positions of frequency detunings.

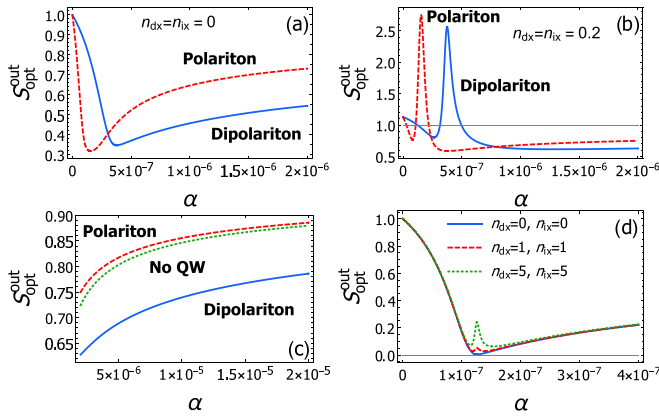


FIG. 15. Variation of the noise spectrum of the dipolariton cavity (and the polariton cavity) as a function of the photonic nonlinearity α and the temperature of the thermal baths in the strong-coupling regime (a) and (b) [$\Omega = J = 2$, $\Delta = 1.05$ (polariton), and $\Delta = 0.1$ (dipolariton)]. (c) Same conditions as (b) and for higher values of nonlinearity. The three systems are represented together: solid line (dipolariton), dashed line (polariton), and dotted line (no quantum well with $\Delta = 0.1$). (d) The weak-coupling regime ($\Omega = J = 0.008$ and $\Delta = 0.15$). In all representations $\gamma = 0.05$, $\kappa = 0.1$, and $\epsilon = 100$.

For weak coupling, the situation is quite different [Figs. 14(c) and 14(d)]. The squeezing effect is obtained only for a quasiresonant excitation. Additionally, we observe that the strongest magnitude effect is realized for $\Omega = J$. This corresponds to the limit of the pulsed tunneling regime.

H. Squeezing and temperature

In this section, we focus on the effect of the temperature of the baths on the stability of the squeezing. First, we assume that our system is at zero temperature. Figure 15(a) represents the spectrum of noise against the nonlinearity coefficient of the two systems. It is shown that in both situations, the systems show similar behaviors. However, the squeezing of light in the polariton cavity reaches its maximum faster than the dipolariton cavity. But, interestingly, the dipolariton system attains the coherent state in a slower way, meaning that the system gives us a good margin for showing a strong squeezing before the light becomes coherent. When thermal excitations take place [Fig. 15(b)], the spectrum of the dipolariton cavity shows also a nonlinearity interval corresponding to high fluctuations. But, differently, the maximum of these fluctuations is attained first by the polariton cavity. After the peak, the squeezing appears again. The same behavior as the zero-temperature case is noticed: The polariton system reaches the coherent state faster. This feature is better illustrated by Fig. 15(c). We note here that the comparison between the three systems is made for detuning values close to that of giving the maximal squeezing of each system.

In the weak-coupling regime, the squeezing effect is very weakly disturbed even at high temperature. In this situation,

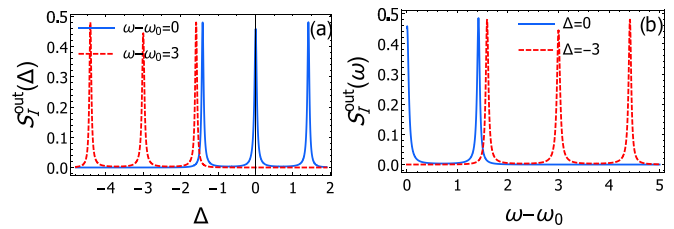


FIG. 16. Intensity power spectrum of the output field in the strong-coupling regime plotted against (a) the detuning and (b) the frequency, for $\alpha = 10^{-8}$, $\Omega = J = 2$, $\gamma = 0.05$, $\epsilon = 100$, $\kappa = 0.1$, and $n_{dx} = n_{ix} = 0.5$.

the polariton cavity showed fluctuations may reach a value of 2.5 in normalized units [Fig. 6(c)]. However, in the dipolariton system, these fluctuations are nonexistent. The only effect of the temperature is a weak decrease of squeezing in a small range of α .

I. Intensity power spectrum

We plot the extracavity intensity power spectrum versus the detuning and the frequency. In Fig. 16(a), at zero frequency, the spectrum consists of three distinct peaks of comparable amplitudes. They are centered around the particular detunings given by $\Delta = 0$ and $\Delta = \pm\Omega/\sqrt{2}$. The symmetrical peaks are then separated by $\sqrt{2}\Omega$. By increasing the frequency, the whole spectrum is also translated towards the negative detunings and keeps the same spacing between peaks. We notice that the peak in the middle corresponds perfectly to $|\Delta| = \omega - \omega_0$. A different aspect from the spectrum of the polariton system is that here the peaks are closer to each other. The variation as a function of the frequency is represented by Fig. 16(b). It is shown that at resonance, the spectrum is formed by two peaks: the first at $\omega - \omega_0 = 0$ and the second placed around $\omega - \omega_0 = \Omega/\sqrt{2}$. For higher detunings, a third peak appears where the peak in the middle corresponds to $\omega - \omega_0 = |\Delta|$. Additionally, the peaks are also closer than for the polariton cavity.

IV. CONCLUSION

We have studied the quantum properties and the photon correlations of the light emitted by a cavity containing a single, then two, coupled quantum wells and interacting with photons resulting from a nonlinear process through a third-order nonlinear medium. By deriving the conditions of the optical bistability in the two systems, we have shown that this regime is reachable in the dipolariton cavity faster than the polariton cavity. Furthermore, dipolaritons induce a *more flexible* squeezing owing to the additional interactions appearing in the dipolariton system. These extra couplings generate a slower attenuation of the nonclassical effect. In addition, it turns out that the weak-coupling regime is favorable to stronger squeezing than the strong coupling in the two systems. In the weak-coupling regime, the two systems have similar behaviors except for a higher resistance against the temperature in favor of the dipolariton system.

- [1] R. W. Boyd, *Nonlinear Optics*, 3rd ed. (Academic/Elsevier, Burlington, 2008).
- [2] H. Schmidt and A. Imamoglu, *Opt. Lett.* **21**, 1936 (1996).
- [3] Y.-F. Xiao, Ş. K. Özdemir, V. Gaddam, C.-H. Dong, N. Imoto, and L. Yang, *Opt. Express* **16**, 21462 (2008).
- [4] I. Fushman and J. Vučković, *Opt. Express* **15**, 5559 (2007).
- [5] U. Khan, B. Amin, K. Ullah, and A. Ullah, *Phys. Lett. A* **383**, 125998 (2019).
- [6] J. Combes and D. J. Brod, *Phys. Rev. A* **98**, 062313 (2018).
- [7] G. Qi, C. Liu-Yong, W. Hong-Fu, and Z. Shou, *Chin. Phys. B* **24**, 040303 (2015).
- [8] I. L. Chuang and Y. Yamamoto, *Phys. Rev. Lett.* **76**, 4281 (1996).
- [9] D. Vitali, M. Fortunato, and P. Tombesi, *Phys. Rev. Lett.* **85**, 445 (2000).
- [10] M. A. Nielsen and I. L. Chuang, *Quantum Computation and Quantum Information* (Cambridge University Press, Cambridge, UK, 2000).
- [11] D. E. Chang, V. Vuletić, and M. D. Lukin, *Nat. Photonics* **8**, 685 (2014).
- [12] Y. R. Shen, *The Principles of Nonlinear Optics* (Wiley-Interscience, New York, 1984).
- [13] C. Flytzanis and J. L. Oudar, *Nonlinear Optics, Devices and Materials* (Springer, Berlin, 1986).
- [14] P. Mandel, S. D. Smidt, and B. S. Wherett, *From Optical Bistability Towards Optical Computing: The EJOB Project* (North-Holland, Amsterdam, 1987).
- [15] O. Sahlen, E. Masseboeuf, M. Rask, N. Nordell, and G. Landgren, *Appl. Phys. Lett.* **53**, 1785 (1988).
- [16] R. Kuszelewicz, J. L. Oudar, J. C. Michel, and R. Azoulay, *Appl. Phys. Lett.* **53**, 2138 (1988).
- [17] S. Zumkley, G. Wingen, G. Borghs, F. Scheffer, W. Prost, and D. Jaeger, in *High Speed Phenomena in Photonic Materials and Optical Bistability*, edited by D. Jaeger (SPIE, 1990), Vol. 1280, pp. 202–208.
- [18] M. T. Tsao, L. Wang, R. Jin, R. W. Sprague, G. Giglioli, H.-M. Kulcke, Y. D. Li, H. M. Chou, H. M. Gibbs, and N. Peyghambarian, *Opt. Eng.* **26**, 41 (1987).
- [19] M. Fukuda, *Optical Semiconductor Devices* (Wiley, New York, 1999).
- [20] Zh. I. Alferov, *Semiconductors* **32**, 1 (1998).
- [21] J. I. Pankove, *Optical Processes in Semiconductors* (Prentice-Hall, Englewood Cliffs, NJ, 1971).
- [22] E. L. Ivchenko, M. A. Kaliteevski, A. V. Kavokin, and A. I. Nesvizhskii, *J. Opt. Soc. Am. B* **13**, 1061 (1996).
- [23] B. Deveaud, *The Physics of Semiconductor Microcavities* (Wiley, New York, 2007).
- [24] K. Vahala, *Optical Microcavities* (World Scientific Publishing, Singapore, 2004).
- [25] E. A. Sete and H. Eleuch, *Phys. Rev. A* **82**, 043810 (2010).
- [26] H. Eleuch, A. Prasad, and I. Rotter, *Phys. Rev. E* **87**, 022916 (2013).
- [27] E. A. Sete, H. Eleuch, and S. Das, *Phys. Rev. A* **84**, 053817 (2011).
- [28] F. Li, Y. Li, Y. Cai, P. Li, H. Tang, and Y. Zhang, *Adv. Quantum Technol.* **2**, 1900060 (2019).
- [29] A. Kavokin and G. Malpuech, *Cavity Polaritons* (Elsevier, Amsterdam, 2003).
- [30] D. Press, S. Götzinger, S. Reitzenstein, C. Hofmann, A. Löffler, M. Kamp, A. Forchel, and Y. Yamamoto, *Phys. Rev. Lett.* **98**, 117402 (2007).
- [31] H. Eleuch, J. M. Courty, G. Messin, C. Fabre, and E. Giacobino, *J. Opt. B: Quantum Semiclass.* **1**, 1 (1999).
- [32] H. Eleuch and R. Bennaceur, *J. Opt. B* **6**, 189 (2004).
- [33] V. Giovannetti, S. Lloyd, and L. Maccone, *Science* **306**, 1330 (2004).
- [34] S. C. Burd, R. Srinivas, J. J. Bollinger, A. C. Wilson, D. J. Wineland, D. Leibfried, D. H. Slichter, and D. T. C. Allcock, *Science* **364**, 1163 (2019).
- [35] H. Yonezawa, D. Nakane, T. A. Wheatley, K. Iwasawa, S. Takeda, H. Arao, K. Ohki, K. Tsumura, D. W. Berry, T. C. Ralph, H. M. Wiseman, E. H. Huntington, and A. Furusawa, *Science* **337**, 1514 (2012).
- [36] P. Cristofolini, G. Christmann, S. I. Tsintzos, G. Deligeorgis, G. Konstantinidis, Z. Hatzopoulos, P. G. Savvidis, and J. J. Baumberg, *Science* **336**, 704 (2012).
- [37] K. Kristinsson, O. Kyriienko, T. C. H. Liew, and I. A. Shelykh, *Phys. Rev. B* **88**, 245303 (2013).
- [38] O. Kyriienko, I. A. Shelykh, and T. C. H. Liew, *Phys. Rev. A* **90**, 033807 (2014).
- [39] K. Kristinsson, O. Kyriienko, and I. A. Shelykh, *Phys. Rev. A* **89**, 023836 (2014).
- [40] A. Seedhouse, J. Wilkes, V. D. Kulakovskii, and E. A. Muljarov, *Opt. Lett.* **44**, 4339 (2019).
- [41] H. Jabri and H. Eleuch, *J. Opt.* **20**, 055201 (2018).
- [42] H. Jabri and H. Eleuch, *J. Opt. Soc. Am. B* **35**, 2317 (2018).
- [43] H. Jabri and H. Eleuch, *J. Opt. Soc. Am. B* **36**, C1 (2019).
- [44] H. Jabri and H. Eleuch, *Ann. Phys. (Berlin)* **531**, 1900253 (2019).
- [45] H. Jabri and H. Eleuch, *Phys. Rev. A* **101**, 053819 (2020).
- [46] H. Jabri and H. Eleuch, *J. Opt. Soc. Am. B* **37**, A9 (2020).
- [47] M. Sargent III, M. O. Scully, and W. Lamb, Jr., *Laser Physics* (Addison-Wesley, Reading, MA, 1974).
- [48] L. Mandel and E. Wolf, *Optical Coherence and Quantum Optics* (Cambridge University Press, Cambridge, UK, 1995).
- [49] E. Giacobino, J. Ph. Karr, G. Messin, H. Eleuch, and A. Baas, *C. R. Phys.* **3**, 41 (2002).
- [50] A. Baas, J. Ph. Karr, H. Eleuch, and E. Giacobino, *Phys. Rev. A* **69**, 023809 (2004).
- [51] G. Messin, J. Ph. Karr, A. Baas, G. Khitrova, R. Houdré, R. P. Stanley, U. Oesterle, and E. Giacobino, *Phys. Rev. Lett.* **87**, 127403 (2001).
- [52] J. Ph. Karr, A. Baas, R. Houdré, and E. Giacobino, *Phys. Rev. A* **69**, 031802(R) (2004).
- [53] A. Fainstein, N. D. Lanzillotti-Kimura, B. Jusserand, and B. Perrin, *Phys. Rev. Lett.* **110**, 037403 (2013).
- [54] D. F. Walls and G. J. Milburn, *Quantum Optics* (Springer, Berlin, 1994).
- [55] G. Messin, J. P. Karr, H. Eleuch, J. M. Courty, and E. Giacobino, *J. Phys.: Condens. Matter* **11**, 6069 (1999).
- [56] H. Eleuch and I. Rotter, *Eur. Phys. J. D* **69**, 229 (2015).
- [57] H. Eleuch and I. Rotter, *Phys. Rev. A* **93**, 042116 (2016).
- [58] M. J. Collett and D. F. Walls, *Phys. Rev. A* **32**, 2887 (1985).
- [59] R. M. Shelby, M. D. Levenson, D. F. Walls, A. Aspect, and G. J. Milburn, *Phys. Rev. A* **33**, 4008 (1986).